2018

Sounds of Failure: Passive Acoustic Measurements of Excited Vibrational Modes

Theodore A. Brzinski III
Haverford College, tbrzinski@haverford.edu

Karen E. Daniels

Editors' Suggestion | Featured in Physics

Sounds of Failure: Passive Acoustic Measurements of Excited Vibrational Modes

Theodore A. Brzinski III* and Karen E. Daniels[1]
Department of Physics, North Carolina State University, Raleigh, North Carolina 27695, USA

(Received 25 July 2017; revised manuscript received 13 March 2018; published 25 May 2018)

Granular materials can fail through spontaneous events like earthquakes or brittle fracture. However, measurements and analytic models which forecast failure in this class of materials, while of both fundamental and practical interest, remain elusive. Materials including numerical packings of spheres, colloidal glasses, and granular materials have been known to develop an excess of low-frequency vibrational modes as the confining pressure is reduced. Here, we report experiments on sheared granular materials in which we monitor the evolving density of excited modes via passive monitoring of acoustic emissions. We observe a broadening of the distribution of excited modes coincident with both bulk and local plasticity, and evolution in the shape of the distribution before and after bulk failure. These results provide a new interpretation of the changing state of the material on its approach to stick-slip failure.

DOI: 10.1103/PhysRevLett.120.218003

The framework provided by the jamming transition [1–3] has highlighted the extent to which granular and other amorphous systems share certain properties: spatially and dynamically heterogeneous response to stress, structural disorder, and inhomogeneous force transmission. While the onset of rigidity in jammed materials shares features with standard second-order phase transitions, jamming differs from other such transitions by its lack of a diverging structural length scale. Although jammed systems are not necessarily thermal, it has been observed that the density of vibrational modes $D(\omega)$ remains an important descriptor of the state of the system. In particular, an excess of low-frequency modes develops on the approach to the jamming transition [4,5] and the onset of plasticity [6]. Indeed, these excess low-frequency modes have been observed in experiments in colloidal systems [7,8] as well as granular materials [9,10].

As such, both experiments and simulations tantalizingly suggest that information about the rigidity of a system might be encoded within $D(\omega; t)$ as the system evolves under external loading (thus, the notation to denote its values at a specific time t). $D(\omega; t)$ is a particularly attractive metric since the passive recording of acoustic emissions provides a noninvasive method of reporting changes in the state of the system and does not require visual access to the system. For example, embedded sensors have long been used for nondestructive evaluation of engineered structures [11,12], and have also successfully identified precursors in volcanic systems [13].

One practical method for measuring $D(\omega; t)$ has been to take advantage of the relationship between the particle velocity autocorrelation function and the density of vibrational modes [14,15]. Recent experiments on a quasi-2D granular packing have used this relationship to establish a connection between acoustic modes and the jamming framework [10]. The procedure is to measure the velocity autocorrelation function

$$C_v(\tau; t) \equiv \frac{\sum v_k(t+\tau) v_k(t)}{\sum v_k(t) v_k(t)}, \tag{1}$$

which is a function of both time (t) and lag time (τ). Here, $v_k(t)$ is the velocity time series measured using the kth of many particle-scale piezoelectric sensors; the sums over k cover all sensors in the system. The density of vibrational modes is then given by [10]

$$D(\omega; t) = \int_0^\infty C_v(\tau; t) \cos(2\pi\omega\tau) d\tau. \tag{2}$$

This approach succeeds even for measurements over a small subset of the particles, recovering the expected Debye scaling for crystalline granular materials as well as the expected excess of low-ω modes in both amorphous and crystalline systems as the confining pressure was reduced.

Our experiments are inspired by prior work on slowly loaded granular materials, from which it is known that (1) particle-scale rearrangements both precede and follow failure events [16], and (2) acoustic emissions and microslips show an exponential increase in their rate of occurrence leading up to a failure event [17,18] and have been shown to encode information about the internal strength of the material [19]. Here, we measure the acoustic emissions during the lead up to failure, and associate changes in the observed $D(\omega; t)$ with the approach to failure. In doing so, we provide a new means of acoustic monitoring. Unlike spectral power measurements, which capture the distribution of acoustic power among modes of different frequencies, the approach we introduce is effectively a measurement of the number of modes which are excited,

regardless of the excitation amplitude. To differentiate from the actual density of vibrational modes, we denote this measurement as the density of excited modes, $D_{\mathrm{ex}}(f;t)$, where f replaces ω as frequency. As far as we know, there are no theoretical expectations for the behavior of D_{ex}; what follows is an empirical exploration.

Our experiment, depicted in Figs. 1(a)–1(c), comprises an annulus with an outer wall of diameter 66.75 cm and an inner wall of diameter 30.5 cm. The system is filled with a single layer of approximately 8000 grains. The grains are a 60∶40 mixture of 5.6 mm circular and 4.9 by 6.9 mm elliptical disks to prevent crystallization. All grains are milled from PhotoStress Plus PS-3 polymer from the Vishay Measurements Group with a bulk elastic modulus of 0.21 GPa. The granular material is sheared at a rate of one rotation per hour via a torsion spring [pictured in Fig. 1(b)] with a stiffness of 0.85 N m/rad and maximum compression of 26°, corresponding to a torque of 0.39 N m.

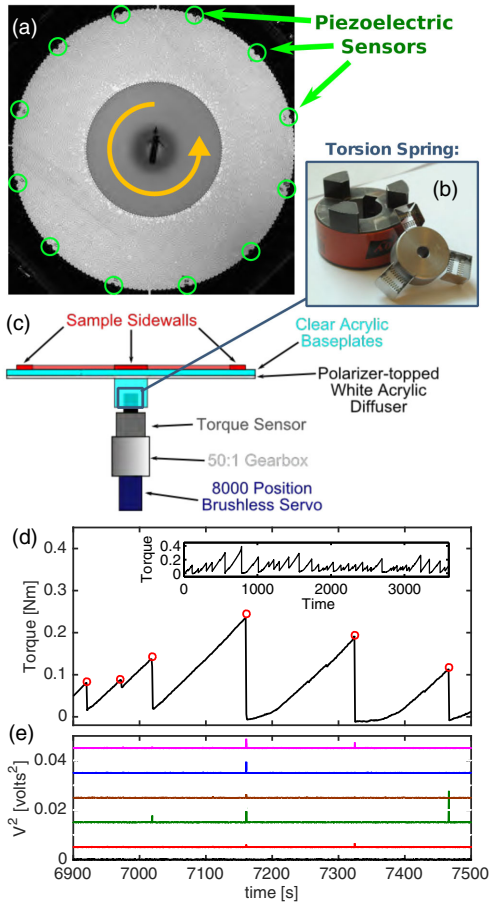

FIG. 1. (a) Top view of the annular shear cell, with piezoelectric sensors and moving (inner) wall. (b) Drive shaft coupling with Hookean torsion spring. (c) Schematic side view illustrating the details of the drive system. (d) Sample torque data over the course of ten minutes and (inset) one hour. Red circles identify slips. (e) Sample measurements of the voltage squared, $V^2(t)$, measured for five piezoelectric sensors, vertically offset and plotted on the same time axis as (d).

Twelve (12) piezoelectric sensors, which are embedded in the outer wall, produce a voltage proportional to any compressive force they experience, thus registering a measurement of the acoustic emissions of the granular material. During an experiment, the driving torque [Fig. 1(d)] and acoustic emissions [(Fig. 1(e)] of the system are continuously measured via a torque sensor (Cooper Instruments) and acoustic sensors (detailed in [20]).

This driving produces intermittent stick-slip failure events, apparent as the sawtooth features in Fig. 1(d). The loading (stick) phase corresponds to the compression of the torsional spring, and when the applied torque surpasses the strength of the granular material, failure (slip) occurs. Empirically, after an initial transient, the frequency of slips remains close to 1 slip/minute. The data presented here were all collected in this steady state over the course of 23 hours. The full dataset of 1165 slip events are aperiodic and span a broad range of torque and time scales [see the inset in Fig. 1(d)], indicating substantial heterogeneity in the material strength and degree of deformation. Despite the spatiotemporal heterogeneity, the slip durations exhibit a relatively narrow distribution with a mean of 0.65 ± 0.14 s. This slipping timescale is well-separated from the interslip (quiescent) timescale: more than 80% of slips, are preceded and followed by quiescent periods of 30 seconds or more. We focus our analysis on the subset of these 887 slips to isolate the effects of individual events.

An illustration of the typical intermittency of the acoustic emissions is provided in Fig. 1(e); each trace is the power from one piezoelectric sensor. We observe that the largest emissions always coincide with slips. Importantly, the converse is not the case: not every slip produces a voltage spike in every sensor. This behavior arises because the force chains cause spatial heterogeneities in acoustic transmission [20]. The typical rms voltage during quiescent periods (without large torque drops) is 2.0 mV, the noise floor of our data acquisition hardware is 1.34 mV, and emission events can produce spikes as much as 3 orders of magnitude higher. In this Letter, we investigate the low-amplitude emissions during the largely quiescent periods between these slips.

We analyze the evolution of the density of excited states, $D_{\mathrm{ex}}(f;t-t_i)$, by the following procedure: for each sensor and slip event occurring at time t_i, we divide the voltage time series into 61 1 s intervals centered around t_i; we integrate the voltage over each interval to obtain the sensor velocities in arbitrary units; we calculate $D_{\mathrm{ex}}(f)$ via Eqs. (1) and (2) [14,15] (see Supplemental Material [21]); we plot this quantity as a function of frequency (f) and $(t-t_i)$ in modograms. Sample modograms for four events are shown in Fig. 2(b). One prominent feature is that a broad range of modes is excited during each slip $(t=t_i)$. However, similar increases in excited modes are also observed at times before and after the slips; these features

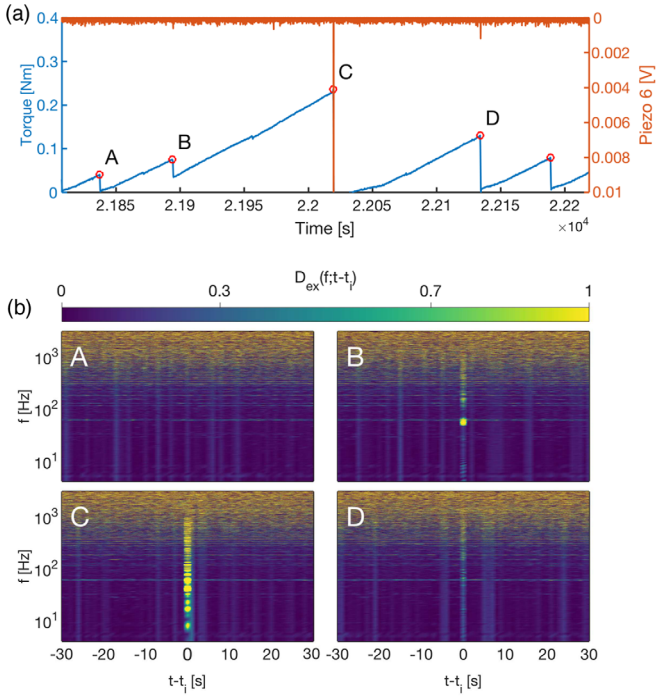

FIG. 2. (a) 400 s of torque (blue) and voltage (red) measurements from one piezoelectric sensor. Five slips are labeled with red circles. (b) Sample modograms showing the density of excited modes $D_{\mathrm{ex}}(f;t-t_i)$ for an interval of ± 30 s centered on each of the four labeled slips (A)–(D).

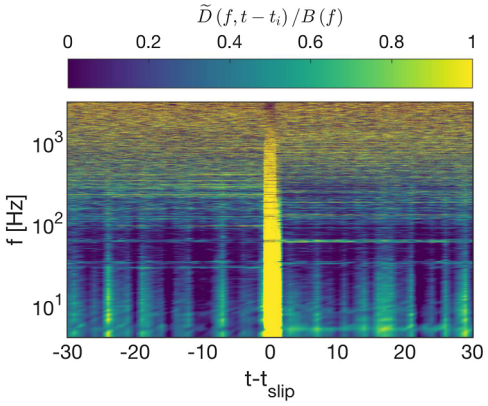

FIG. 3. Average modograms $\tilde{D}_{\mathrm{ex}}(f;t-t_i)$, taken over 887 slips and 12 sensors and normalized by the sensor- and time-averaged density of excited states, $B(f)$.

are visible as bright vertical bands in Fig. 2(b). We also observe that the overall density of excited modes appears to be relatively flat over nearly three decades (Hz to kHz), rising only at the highest frequencies in this range. Finally, we observe several persistent frequencies which appear as horizontal lines. While the 60 Hz peak is of electronic origin, the others are likely due to acoustic noise such as from the drive system or building noise. These noise peaks will be filtered out in the later stages of analysis.

We begin by focusing on the vertical bands visible in Fig. 2(b). Each of these bands represents a time at which a single piezoelectric sensor detected an increase in the number of excited vibrational modes over a broad range of frequencies. Some of these vertical bands correspond to global slip events ($t = t_i$), but most are detected due to local rearrangements which happened to occur close to a particular sensor. The local nature of these detections is reinforced by the observation that modograms from different sensors do not all record increases [as also seen in Fig. 1(e)]. The ability to measure the $D_{\mathrm{ex}}(f;t-t_i)$ from either low- or high-amplitude slip events is crucially important to this method. While the low-amplitude events are too small to cause a global slip event, some of them are, nonetheless, large enough to be detected as they travel through the granular material and, thereby, leave a record of the state of the material. As we shall see below, the information they transmit reveals the changing state of the material.

In order to reduce the impact of noise in the density of excited modes, we construct the average modogram $\tilde{D}_{\mathrm{ex}}(f;t-t_i) \equiv \langle D_{\mathrm{ex}}(f;t-t_i)\rangle_{i,k}$, where i is an index over the 887 detected slips separated by at least 30 s from the adjacent slips, and k is an index over the 12 sensors. To highlight the relative changes this quantity exhibits in response to failure and to suppress persistent electronic or physical resonances, we normalize $\tilde{D}_{\mathrm{ex}}$ by the sensor- and time-averaged density of excited states, $B(f) = \langle \tilde{D}_{\mathrm{ex}}(f;t-t_i)\rangle_{t\neq t_i}$ to obtain the rescaled modogram shown in Fig. 3.

This normalized average modogram exhibits features similar to the fluctuations observed in Fig. 2, but now, the vertical streaks result from the average behavior over many slips and sensors. The remaining heterogeneity indicates that 887 slips were an insufficient quantity of data to eliminate the temporal heterogeneity associated with localized plasticity. Even within this noisy signal, however, there emerge clear differences between the preslip and postslip portions of this modogram.

To characterize the changes in the slip- and sensor-averaged $\tilde{D}_{\mathrm{ex}}$, we calculate the first four moments of that quantity. These are best considered as empirical shape parameters, since there is no prediction for the shape of $\tilde{D}_{\mathrm{ex}}$, and our dynamic range may capture only a portion of the distribution. Nonetheless, a clear signal is evident in these quantities (Fig. 4). We find that the mean frequency (a) gradually grows during the preslip phase, and then, suddenly decreases from 1.60 to 1.59 kHz (less than 1%) in response to slips. This effect is accompanied by a small increase in the variance (b) If our dynamic range captures most of the excited modes, these changes are consistent with a broadening of $\tilde{D}_{\mathrm{ex}}(f)$ in response to failure, with excited modes arising at lower-frequencies. Since the internal stress in the granular material is lower after a slip [see Fig. 1(d)], these observations are consistent with the observations of failure of the force chain network [22] and

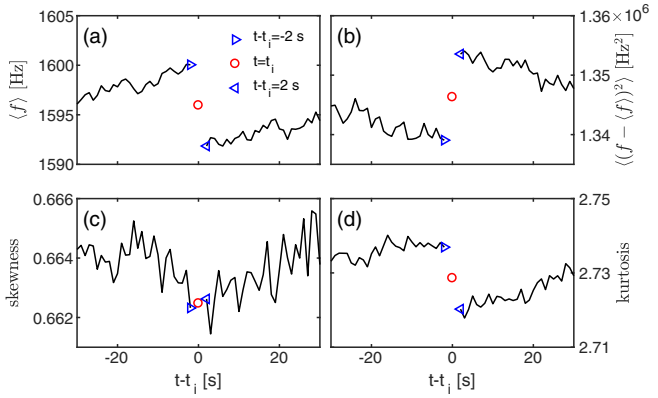

FIG. 4. The four moments of $\tilde{D}_{\mathrm{ex}}(f; t - t_i)$, calculated at fixed times preslip and postslip: (a) mean frequency, (b) variance, (c) skewness, and (d) kurtosis. The red "circles" indicates the time of the slip (data point omitted for clarity). The right- and left-pointing cyan triangles indicate the values immediately before and after the slip.

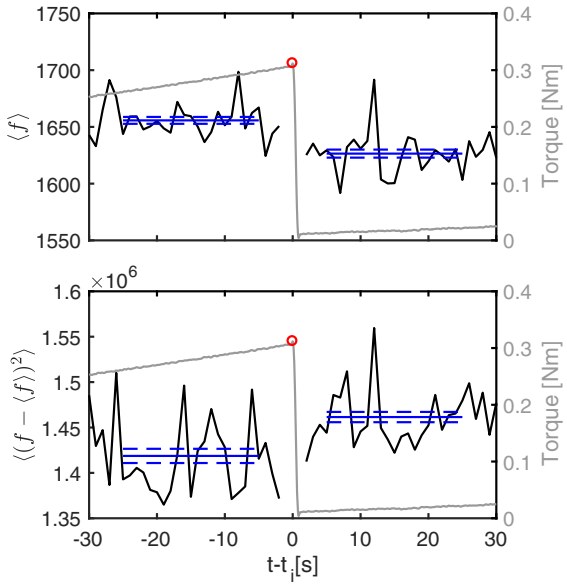

FIG. 5. (top) $\langle f \rangle$ and (middle) $\langle (f - \langle f \rangle)^2 \rangle$ for $D_{\mathrm{ex}}(f; t - t_i)$ for a single slip, measured by a single sensor. The solid blue lines show the mean values for the first and last 28 seconds, respectively, and dashed lines show the 95% confidence in these means. In both plots, the torque is plotted on the right axis in light grey, with the slip indicated by a red circle. (bottom) The success rates for which we observed statistically significant discontinuities in the mean, variance, and kurtosis in f for D_{ex} as measured by a single sensor and at a time coincident with a slip. Boldface values are those that match the sign of the average changes.

emergence of excess low-frequency modes [10] at smaller confining stresses.

We also observe similarly clear, but still small, signals in the higher central moments of $\tilde{D}_{\mathrm{ex}}$: a weak minimum in skewness and a 1% drop in the kurtosis [panels (c)–(d), respectively]. We find a skewness of 0.66, which means low-frequency modes are more common than high-frequency modes. The kurtosis close to 3 indicates $\tilde{D}_{\mathrm{ex}}$ is neither particularly heavy nor weak tailed.

Finally, we consider D_{ex} as a possible metric for characterizing single-slip, single-sensor measurements. In Fig. 5, we examine a characteristic example for a period centered on a single slip. $\langle f \rangle$ (top) and $\langle (f - \langle f \rangle)^2 \rangle$ (middle) of the excited modes, calculated based on a single sensor, are plotted against $t - t_i$. To highlight the stepwise change at $t = t_i$, we additionally plot the mean $\pm 2\sigma$ as horizontal lines during the preslip and postslip times, and plot the torque on the right axis in both plots. As for the ensemble-averaged data (Fig. 4), we observe a significant drop in $\langle f \rangle$ coincident with the slip at $t = t_i$ accompanied by a rise in the variance. We perform this same analysis for all slips that are well-separated in time, for all 12 piezos, for $887 \times 12 = 10\,644$ sets of statistics of the type shown in Fig. 5. The results of this analysis are summarized in the table in Fig. 5 (bottom). We find that single sensor measurements are consistent with the trends depicted in Fig. 4, as emphasized by the boldface type in Fig. 5 (bottom). Importantly, some slips will produce a detectable signal in these metrics for only one or a subset of sensors. Moreover, some slips produce no signal at any sensor due to the dissipative nature of the system and because the 12 sensors, each approximately 5 mm wide, cover less than 1% of the length of the perimeter.

The analysis we present here represents an important step in connecting passive acoustic measurements directly to the state of the material. While acoustic emissions have previously been known to coincide with the failure of granular media, our method provides a new capability: assessment of the progress of a system en route to failure. The shift observed in moments of the occupancy of vibrational modes is consistent with observations that granular systems under less stress exhibit an excess of floppy, low-frequency modes [10], and can be connected more broadly to similar observations in jammed solids as the volume fraction is reduced [7,8,23] and as shear progresses [24]. Our results indicate promise for predictive forecasting of failure in slowly sheared, disordered systems. However, any approach to forecasting of this sort is most likely to be probabilistic rather than deterministic: $\tilde{D}_{\mathrm{ex}}$ may signal an increased likelihood for an event, particularly with better sensor coverage where passive measurements may more completely reveal the features of the density of vibrational modes. These techniques also provide a route for improved characterization of the vibrational properties of disordered materials.

Assessing the internal stress state of a granular system is notoriously difficult: photoelastic, optical, and tomographic techniques [25–27] require specialized materials or slow scanning times to make quantitative measurements of internal stresses. We have found that the density of excited vibrational modes $D_{\mathrm{ex}}(f)$ appears to provide a new

technique for reporting the internal stress in the system which does not require optical access, and can be applied to 3D systems with fast measurement times. Importantly, this method does not require acoustic driving, which risks triggering a failure in materials near threshold, and should work on a variety of materials. Furthermore, this analysis is largely independent of the details of the sensor mechanism, so an obvious next step is to test the approach with seismic data.

This work was supported by NSF Grant No. DMR-1206808 and the James S. McDonnell Foundation. We thank Paul Johnson, Craig Maloney, Corey O'Hern, and Eli Owens for helpful discussions, and Cross Automation for technical assistance with our motion control needs.

*Present Address: Department of Physics and Astronomy, Haverford College, Haverford, Pennsylvania 19041, USA. tbrzinski@haverford.edu

[1] A. J. Liu and S. R. Nagel, *Jamming and Rheology: Constrained Dynamics on Microscopic and Macroscopic Scales* (Taylor & Francis, London, 2001).
[2] A. J. Liu and S. R. Nagel, Annu. Rev. Condens. Matter Phys. **1**, 347 (2010).
[3] M. van Hecke, J. Phys. Condens. Matter **22**, 033101 (2010).
[4] C. S. O'Hern, L. E. Silbert, A. J. Liu, and S. R. Nagel, Phys. Rev. E **68**, 011306 (2003).
[5] M. Wyart, Ann. Phys. (Paris) **30**, 1 (2005).
[6] A. Tanguy, B. Mantisi, and M. Tsamados, Europhys. Lett. **90**, 16004 (2010).
[7] A. Ghosh, V. K. Chikkadi, P. Schall, J. Kurchan, and D. Bonn, Phys. Rev. Lett. **104**, 248305 (2010).
[8] K. Chen, W. G. Ellenbroek, Z. Zhang, D. T. N. Chen, P. J. Yunker, S. Henkes, C. Brito, O. Dauchot, W. van Saarloos, A. J. Liu, and A. G. Yodh, Phys. Rev. Lett. **105**, 025501 (2010).
[9] C. Brito, O. Dauchot, G. Biroli, and J.-P. Bouchaud, Soft Matter **6**, 3013 (2010).
[10] E. T. Owens and K. E. Daniels, Soft Matter **9**, 1214 (2013).
[11] H. Dunegan, D. Harris, and C. Tatro, Eng. Fract. Mech. **1**, 105 (1968).
[12] A. Nair and C. S. Cai, Engineering structures **32**, 1704 (2010).
[13] G. Paparo, G. P. Gregori, U. Coppa, R. de Ritis, and A. Taloni, Ann. Geophys. **45**, 401 (2002).
[14] J. M. Dickey and A. Paskin, Phys. Rev. **188**, 1407 (1969).
[15] T. Keyes, J. Phys. Chem. A **101**, 2921 (1997).
[16] S. Nasuno, A. Kudrolli, and J. P. Gollub, Phys. Rev. Lett. **79**, 949 (1997).
[17] A. Garcimartín, A. Guarino, L. Bellon, and S. Ciliberto, Phys. Rev. Lett. **79**, 3202 (1997).
[18] P. A. Johnson, B. Ferdowsi, B. M. Kaproth, M. Scuderi, M. Griffa, J. Carmeliet, R. A. Guyer, P. Y. Le Bas, D. T. Trugman, and C. Marone, Geophys. Res. Lett. **40**, 5627 (2013).
[19] B. RouetLeduc, C. Hulbert, D. C. Bolton, C. X. Ren, J. Riviere, C. Marone, R. A. Guyer, and P. A. Johnson, Geophys. Res. Lett. **45**, 1321 (2018).
[20] E. T. Owens and K. E. Daniels, Europhys. Lett. **94**, 54005 (2011).
[21] See Supplemental Material at http://link.aps.org/supplemental/10.1103/PhysRevLett.120.218003 for typical examples of the intermediate stages of analysis, and typical spectrograms of our acoustic emissions.
[22] D. Howell, R. P. Behringer, and C. Veje, Phys. Rev. Lett. **82**, 5241 (1999).
[23] L. E. Silbert, A. J. Liu, and S. R. Nagel, Phys. Rev. Lett. **95**, 098301 (2005).
[24] M. L. Manning and A. J. Liu, Phys. Rev. Lett. **107**, 108302 (2011).
[25] T. S. Majmudar and R. P. Behringer, Nature (London) **435**, 1079 (2005).
[26] N. Brodu, J. A. Dijksman, and R. P. Behringer, Nat. Commun. **6**, 6361 (2015).
[27] R. C. Hurley, S. A. Hall, J. E. Andrade, and J. Wright, Phys. Rev. Lett. **117**, 098005 (2016).